

Supporting the Engineering Analysis of Offshore Wind Turbines Through Advanced Soil-Structure 3D Modelling

Corciulo, Simone; Zanolli, Omar; Pisano, Federico

DOI

[10.1115/OMAE2017-62469](https://doi.org/10.1115/OMAE2017-62469)

Publication date

2017

Document Version

Final published version

Published in

Torgeir Moan Honoring Symposium

Citation (APA)

Corciulo, S., Zanolli, O., & Pisano, F. (2017). Supporting the Engineering Analysis of Offshore Wind Turbines Through Advanced Soil-Structure 3D Modelling. In *Torgeir Moan Honoring Symposium: Proceedings of the 36th International Conference on Ocean, Offshore and Arctic Engineering* (Vol. 9). Article OMAE2017-62469 (ASME Conference Proceedings; Vol. 9). ASME.
<https://doi.org/10.1115/OMAE2017-62469>

Important note

To cite this publication, please use the final published version (if applicable). Please check the document version above.

Copyright

Other than for strictly personal use, it is not permitted to download, forward or distribute the text or part of it, without the consent of the author(s) and/or copyright holder(s), unless the work is under an open content license such as Creative Commons.

Takedown policy

Please contact us and provide details if you believe this document breaches copyrights. We will remove access to the work immediately and investigate your claim.

OMAE2017-62469

SUPPORTING THE ENGINEERING ANALYSIS OF OFFSHORE WIND TURBINES THROUGH ADVANCED SOIL-STRUCTURE 3D MODELLING

Simone Corciulo & Omar Zanoli
Geo & Structures
D'Appolonia S.p.A.
via Martiri di Cefalonia 2 – 20097
San Donato Milanese (Italy)

Federico Pisanò*
Geo-Engineering Section/Offshore Engineering Section
Delft University of Technology
Stevinweg 1 – 2628 CN
Delft (The Netherlands)
Email: F.Pisano@tudelft.nl

ABSTRACT

Monopiles are at present the most widespread foundation type for offshore wind turbines (OWTs), due to their simplicity and economic convenience. The current trend towards increasingly powerful OWTs in deeper waters is challenging the existing procedures for geotechnical design, requiring accurate assessment of transient soil-monopile interaction and, specifically, of the associated modal frequencies.

In this work, advanced 3D finite element (FE) modelling is applied to the dynamic analysis of soil-monopile-OWT systems under environmental service loads. Numerical results are presented to point out the interplay of soil non-linearity and cyclic hydro-mechanical (HM) coupling, and its impact on transient response of the system at increasing load magnitude. It is shown how the lesson learned from advanced modelling may directly inspire simplified, yet effective, spring models for the engineering dynamic analysis of OWTs.

INTRODUCTION

An obvious relationship links nowadays the gradual depletion of hydrocarbon reserves and the need for clean/sustainable energy sources. Since the late 1990s, significant wind energy programmes have been started in several European countries to install large offshore wind farms (see e.g. Fig. 1). According to Wind Europe (formerly European Wind Energy Association),



FIGURE 1. KENTISH FLATS OFFSHORE WIND FARM (UK).

UK is currently the largest offshore wind market and accounts for over 40% of installed global capacity, while 3 GW of new offshore wind capacity came online in Europe in 2015, 75% of which in Germany [1]. At present, more than half OWTs in Europe are supported by monopile foundations, whose design/installation relies upon simplified procedures currently being challenged by the trend towards deeper waters.

The dynamic response of OWTs is governed to a large extent by the cantilever-like eigenmode associated with the first natural frequency f_0 of the system. Its identification is a major design issue [2], and relates to preventing structural resonance under the vibrations induced by environmental loads and blade rotation. Profound understanding of dynamic soil-monopile interaction is

*Address all correspondence to this author.

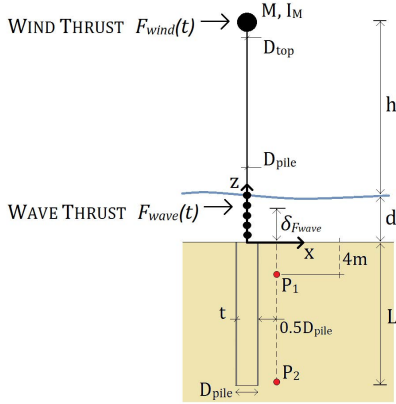


FIGURE 2. REFERENCE 5MW OWT AND FOUNDATION SYSTEM.

therefore essential for effective design, to be achieved through an accurate evaluation of f_0 . In this respect, monopiles have been found to behave quite differently from the slender piles of typical offshore platforms, so that the accuracy of standard $p-y$ curves when applied to large diameter monopiles is questionable [3].

In agreement with the research agenda by the European Academy of Wind Energy [4], this work aims to complement the current approaches to monopile design by gaining insight from the 3D finite element (FE) analysis of non-linear geotechnical systems. The OpenSees simulation platform [5] and an advanced soil constitutive model are used to capture the interplay of cyclic effects and hydro-mechanical (HM) coupling in soil-monopile dynamic interaction [6, 7]. The outcomes of advanced FE simulations are finally exploited to inspire simplified, yet sound, engineering models.

3D FE MODELLING OF SOIL-MONOPILE-OWT

The OWT system modelled in this study is consistent with the reference 5 MW OWT defined by Jonkman et al. [8]. A complete description of all numerical modelling aspects, only summarised here, is available in [7].

Structural set-up

Figure 2 depicts the reference system under consideration: the monopile foundation is wished-in-place into the soil, while the tapered superstructure is subjected to wind/wave thrust forces (F_{wind} and F_{wave}) and modelled as a 1D Timoshenko beam (geometric/inertial properties are linearly varying along the elevation). The structural model includes both mass (M) and rotational inertia (I_M) of the turbine, as well as discrete added masses (m_w) mimicking the presence of the sea water around the structure. All structural specifications are listed in Tab. 1.

TABLE 1. STRUCTURAL PROPERTIES OF THE OWT-MONOPILE SYSTEM.

h	d	L	$D_{pile-top}$	t	M	I_M	m_w
[m]	[m]	[m]	[m]	[-]	[te]	[te · m ²]	[te]
90	20	20	5–3	0.01D	350	2600	785

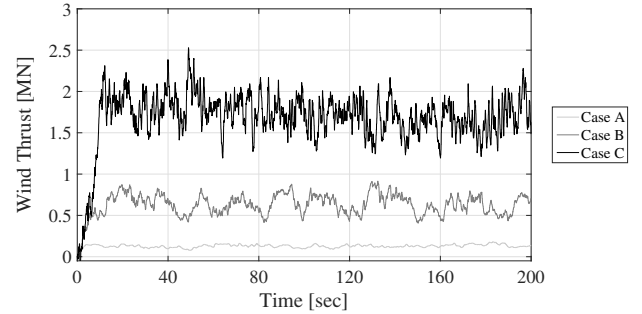


FIGURE 3. WIND THRUST TIME HISTORIES.

Environmental loads

Three loading scenarios (cases A, B and C) are set to represent the environmental loads corresponding with the wind speeds of 5 m/s (case A), 12 m/s (case B) and 20 m/s (case C). The F_{wind} time histories in Fig. 3 are obtained by converting anemometric records from an instrumented OWT in the Irish Sea through Blade Element Momentum (BEM) theory [9]. F_{wave} time histories are derived from the given wind speed via the spectral formulation of Pierson and Moskowitz [10]; the conversion from wave spectra to thrust forces is performed via the well-known Morison equation [11, 12], resulting in mono-harmonic loading with increasing amplitude and period at larger wind speed (Fig. 4). The present simplified modelling of environmental loads does not account for air-rotor interaction, so that the aerodynamic component of the global operational damping is neglected.

Formulation and FE solution of soil dynamic problems

The so-called $u-p$ formulation is adopted to describe the dynamic HM response of the soil. This formulation stems from the assumption of negligible soil-fluid relative acceleration, which suits typical offshore applications with wind/wave loading frequencies lower than 0.5 Hz.

Geometrical and loading symmetries are exploited to reduce the computational burden. The halved soil domain in Fig. 5 is discretised by using approximately 6000 8-node two-phase bricks element of the SSP (Stabilized Single Point) type [13]. These equal-order elements can prevent spurious pore pressure oscillations close to the undrained-incompressible limit

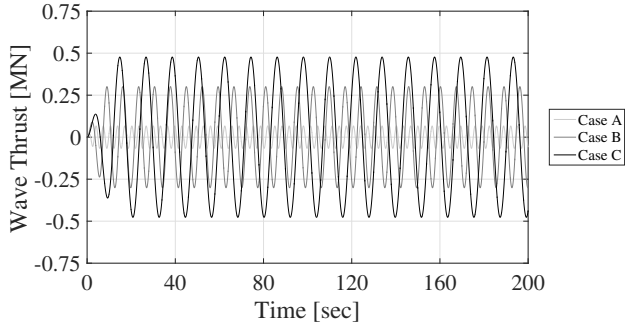


FIGURE 4. WAVE THRUST TIME HISTORIES.

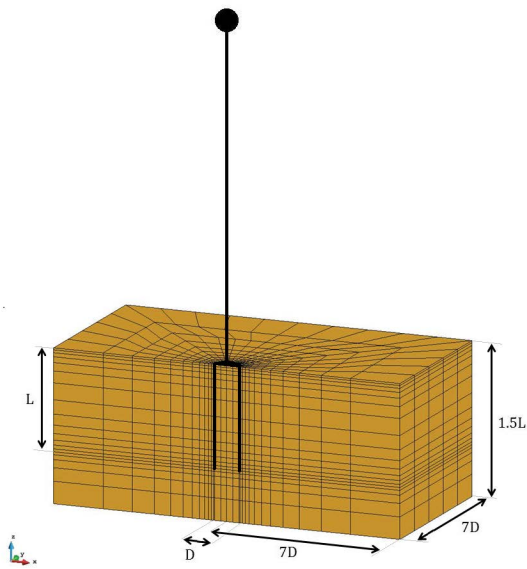


FIGURE 5. FE DISCRETIZATION OF THE SOIL DOMAIN.

through a non-residual-based stabilization. Conversely, the steel monopile is modelled by means of one-phase SSP solid elements.

The implicit Newmark algorithm ($\beta = 0.6$, $\gamma = (\beta + 0.5)^2/4$) is employed for time marching in combination with explicit forward Euler integration of soil constitutive equations.

Sand cyclic HM behaviour

A homogeneous deposit of medium dense silica sand is considered as foundation soil. Sand cyclic behaviour is reproduced via the UCSD08 multi-surface plasticity model [14], able to reproduce pressure-sensitiveness, volumetric-deviatoric coupling and cyclic hysteresis. Table 2 reports the UCSD08 soil parameters calibrated against triaxial test results performed on sand specimens from offshore Myanmar (sampled 20 m below the mudline). A thin layer as thick as 4% of monopile diameter with

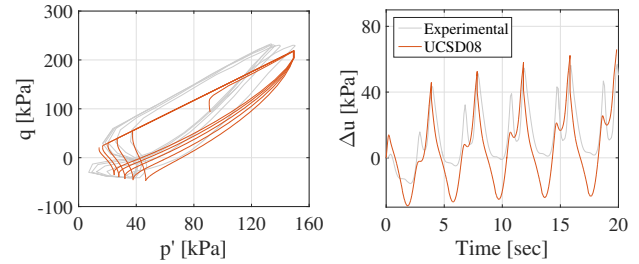


FIGURE 6. UCSD08 SIMULATION VS CYCLIC TRIAXIAL TEST DATA (COURTESY OF D'APPOLONIA S.P.A).

TABLE 2. UCSD08 SAND PARAMETERS ($D_R \approx 60\%$, $\rho = 1.8 \text{ Mg m}^{-3}$).

G_r	K_r	p'_r	ϕ'	γ_{max}	ϕ_{PT}	γ_{smax}
[MPa]	[MPa]	[kPa]	[deg]	[%]	[deg]	[%]
100	170	100	35.5	8.5	31	0.0
c_1	c_2	c_3	d_1	d_2	d_3	p'_y
[-]	[-]	[-]	[-]	[-]	[-]	[-]
0.125	0.5	1	0.25	3.9	5.7	1.95

reduced friction and phase transformation angles is inserted to model soil-monopile interface, and a permeability $k = 10^{-5} \text{ m/s}$ is assumed. Figure 6 exemplifies the quite satisfactory agreement between UCSD08 simulations and experiments in terms of $q - p'$ stress path and excess pore pressure accumulation.

RESPONSE TO ENVIRONMENTAL LOADING

This sections summarises the outcomes of 3D soil-monopile-OWT dynamic simulations for the above-mentioned loading scenarios (cases A, B, C). All considered time histories last 200 s and require approximately 500 hours of sequential calculation on a 3.70 GHz Intel Xeon CPU. The following results represent a step forward compared to the shorter simulations recently performed by Corciulo *et al.* [7].

Soil-monopile interaction

Figures 7-8 illustrate the mechanical response of the soil (shear stress-strain curves and effective stress paths) at the two control points P_1 and P_2 indicated in Fig. 2; the colorbars on the side represent time elapsing over the 0-200 s interval.

The stress-strain plots in Fig. 7 point out clearly the increase in soil non-linearity mobilised at increasing load level. Indeed, while a nearly linear response is produced in case A (*weak vibra-*

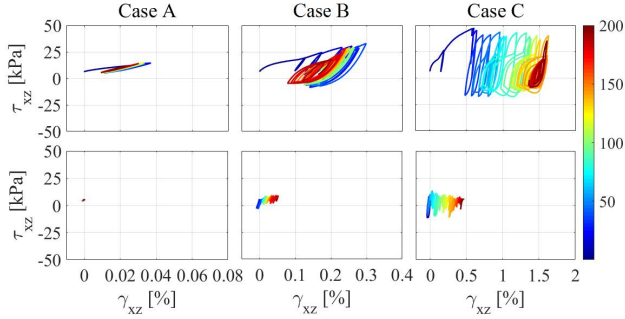


FIGURE 7. SHEAR STRESS-STRAIN RESPONSE AT THE POINTS P1 (TOP) AND P2 (BOTTOM) IN FIG. 2. (COLORBAR: 0-200 SEC TIME-TRACKING)

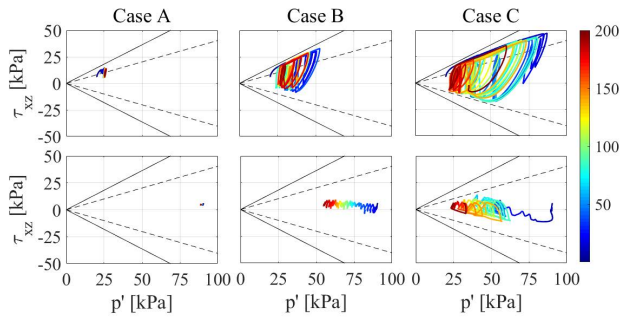


FIGURE 8. SOIL EFFECTIVE STRESS PATHS AT THE POINTS P1 (TOP) AND P2 (BOTTOM) IN FIG. 2 (COLORBAR: 0-200 SEC TIME-TRACKING).

tion case), evident stress-strain hysteresis loops and strain accumulation result in case C (*strong vibration* case). Consistently, the effective stress paths in Fig. 8 show the occurrence of cyclic mobility at shallow soil locations (point P_1): this is associated with the temporary increase in effective confinement p' when the stress path crosses the phase transformation line (dashed lines), due to prevented soil dilation; conversely, no cyclic mobility effects are observed at point P_2 because of the stress path always lying within the phase transformation locus. Variations in effective confinement go hand in hand with the excess pore pressure (Δu) time-plots in Fig. 9. In case C, a general pore pressure accumulation trend is clearly visible as counterpart of the p' reduction in Fig. 8, especially close to the mudline (point P1). Pore pressure build-ups are direct outcome of the interaction between cyclic loading and dynamic consolidation, with an obvious influence of the loading amplitude – sands exhibit low deviatoric-volumetric coupling in the nearly linear, *weak vibration* regime.

Figures 10-11 illustrate the performance of the foundation in terms of horizontal load-displacement ($H - \delta$) and moment-rotation ($M - \theta$) curves at the monopile head (i.e. at mudline), chosen here as global measure of local HM processes through-

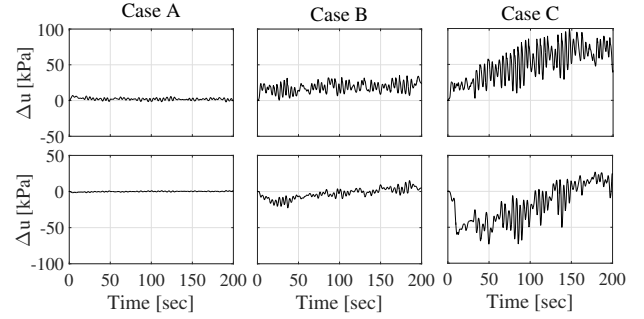


FIGURE 9. TIME EVOLUTION OF EXCESS PORE PRESSURE AT THE POINTS P1 (TOP) AND P2 (BOTTOM) IN FIG. 2.

out the soil domain. The corresponding $H - \delta$ backbone curves from static FE analyses are plotted alongside to highlight the differences between monotonic and cyclic behaviour of the foundation. For each case, equivalent translational (K_L) and rotational (K_R) stiffness values can be identified in combination with a specific load level. Obviously, deriving foundation stiffness from global $H - \delta$ and $M - \theta$ plots does not enable to distinguish compliance and inertial components, although with not dramatic consequences in case of low-frequency loading (Figs. 3-4). Figs. 10–11 suggest the following observations:

- in the transition from *weak* to *strong* vibration a gradual decrease in lateral foundation stiffness is observed as an effect of soil non-linearity – $K_{L,A} = 210 \text{ MN m}^{-1}$, $K_{L,B} = 130 \text{ MN m}^{-1}$, $K_{L,C1} = 100 \text{ MN m}^{-1}$;
- the lateral stiffness is apparently unsteady in case C. After an initial degradation (from $K_{L,C1} = 100 \text{ MN m}^{-1}$ to $K_{L,C2} = 80 \text{ MN m}^{-1}$), stiffness recovery occurs ($K_{L,C3} = 110 \text{ MN m}^{-1}$) towards the end of the time history (see colorbars), possibly due to soil cyclic mobility;
- lateral displacement and rotation are gradually accumulated at the monopile head, with increasing energy dissipation as the load amplitude gets higher;
- the rotational monopile stiffness appears to be less sensitive to soil non-linearity – $K_{R,A} = 52 \text{ GN mrad}^{-1}$, $K_{R,B} = 45 \text{ GN mrad}^{-1} = K_{R,C1}$, $K_{R,C2} = 40 \text{ GN mrad}^{-1}$.

The above points are all relevant to the resulting OWT dynamics and should be taken into account when formulating simplified analysis approaches.

OWT dynamics

Figures 12-13 show the displacement time histories simulated for the monopile head and the OWT hub (cases A, B and C). The increasing vibration amplitude of the OWT hub at larger wind speed is apparent, as well as the gradual displacement accumulation characterising case C above all.

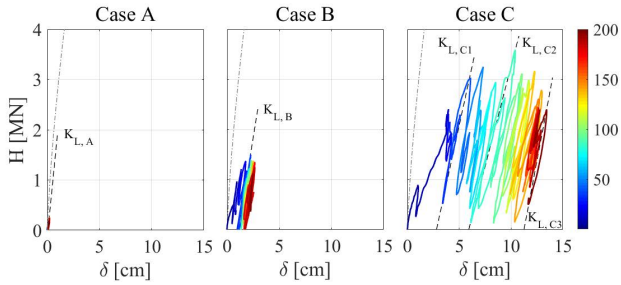


FIGURE 10. HORIZONTAL FORCE-DISPLACEMENT RESPONSE AT THE MONOPILE HEAD (COLORBAR: 0-200 SEC TIME-TRACKING).

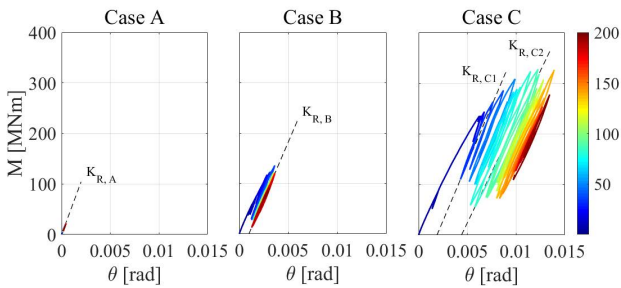


FIGURE 11. HORIZONTAL MOMENT-ROTATION RESPONSE AT THE MONOPILE HEAD (COLORBAR: 0-200 SEC TIME-TRACKING).

The vibrational response of the OWT is also inspected in the frequency domain in Fig. 14. The Frequency Response Function (FRF) of the structure is derived for all loading scenarios from the spectral ratios between Fourier amplitude of the OWT hub velocity and the wind speed history. Such spectral ratios provide here a good representation of the OWT frequency response for two reasons: (i) regardless of non-linear effects, the monoharmonic wave loads in Fig. 4 do never align with any natural frequency of the system; (ii) the typical “noise” in numerical spectral ratios is mitigated by avoiding unnecessary differentiations (for instance to derive the inertial force at the hub).

Figure 14 shows raw spectral ratios (lilac lines) and the more readable results obtained after preliminary low-pass filtering (red lines). The main natural frequency f_0 is also indicated in all FRF plots. Transiting from *weak* (case A) to *strong* (case C) vibration conditions, a reduction in f_0 is caused by the evolution of the monopile stiffness (see Figs. 10–11). However, the f_0 decrease rate with the loading amplitude is not constant, but a slower rate is observed as the wind speed grows higher. It is argued that this interesting outcome arises from the peculiar behaviour of medium-dense/dense sands under closely undrained conditions: they lose shear stiffness at increasing strain amplitude (i.e. wind speed), but also tend to regain stiffness owing to negative excess

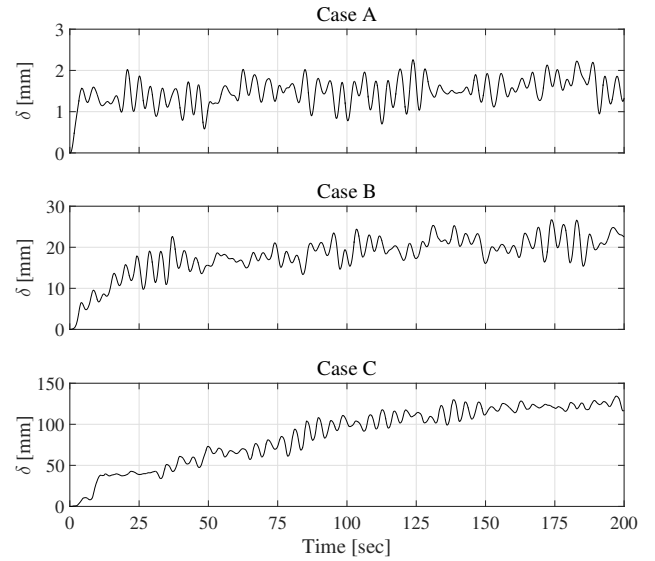


FIGURE 12. HORIZONTAL DISPLACEMENT TIME HISTORIES AT THE MONOPILE HEAD.

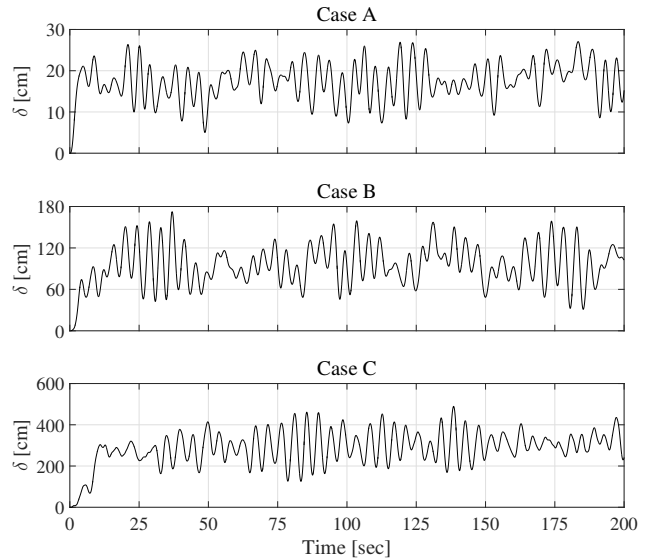


FIGURE 13. HORIZONTAL DISPLACEMENT TIME HISTORIES AT THE OWT HUB.

pore pressures. As a result, undrained dilatancy effects induce higher effective confinement and in turn a recovery of foundational stiffness. As previously mentioned, this aspect is clearly depicted for case C in Fig. 10, where the non-monotonic stiffness variation trend may be regarded as the cause of the steady f_0 value from case B to C.

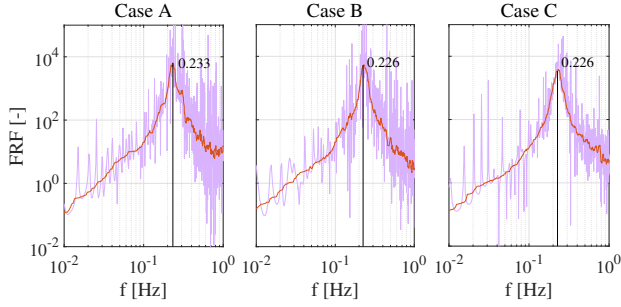


FIGURE 14. OWT RESPONSE IN THE FREQUENCY DOMAIN.

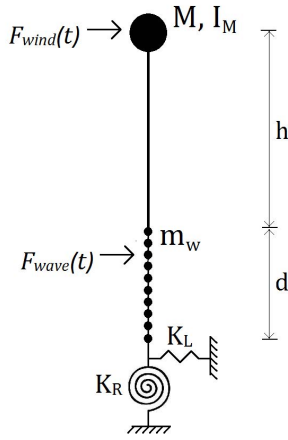


FIGURE 15. SIMPLIFIED OWT MODEL WITH TRANSLATIONAL AND ROTATIONAL SPRING SUPPORTS.

FROM ADVANCED TO ENGINEERING MODELLING

In this section, the findings from advanced FE analyses are exploited to tune engineering spring models for dynamic soil-structure interaction. A simplified version of the model in Fig. 2 is developed according to the sketch in Fig. 15, that is by setting translational and rotational elastic supports in lieu of the 3D soil domain (a similar approach was previously attempted by Adhikari and Bhattacharya [15]). Accordingly, the global stiffness components K_L and K_R defined above need to be calibrated for lumped 3D soil-structure interaction.

For this purpose, three different stiffness calibrations are adopted:

- **Simplified Model 1.** $K_{L,1} = 450 \text{ MN m}^{-1}$ and $K_{R,1} = 56 \text{ GN mrad}^{-1}$, calibrated against the initial branches of static/monotonic $H - \delta$ and $M - \theta$ FE curves;
- **Simplified Model 2.** *weak vibration* cyclic stiffness $K_{L,2} = 210 \text{ MN m}^{-1}$ and $K_{R,2} = 52 \text{ GN mrad}^{-1}$. Note that in general monotonic and dynamic small strain stiffness may not coincide due to HM coupling and inertial effects;

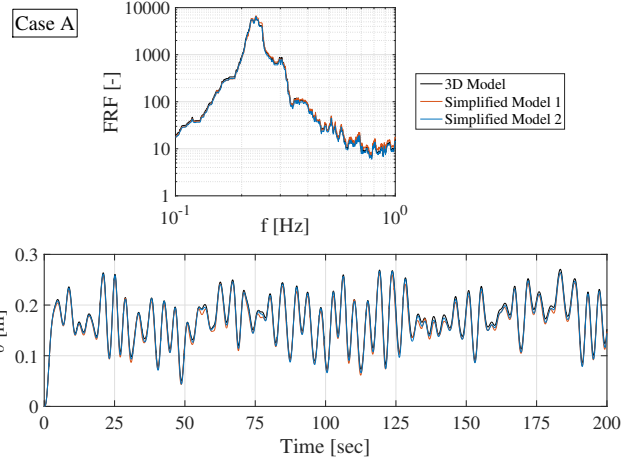


FIGURE 16. COMPARISON BETWEEN 3D AND SPRING MODEL 1-2 SIMULATIONS OF LOADING SCENARIO A.

- **Simplified Model 3.** *strong vibration* cyclic stiffness $K_{L,3} = 90 \text{ MN m}^{-1}$ and $K_{R,3} = 40 \text{ GN mrad}^{-1}$, plus a translational viscous damper (viscous coefficient: $C_D = 20 \text{ MN m}^{-1} \text{ s}$) to capture hysteretic energy dissipation at the dominant oscillation period. The intermediate large oscillation stiffness $K_{L,3}$ is substantially lower than $K_{L,1}$, although it is not the lowest value exhibited during the vibration history C.

Figure 16 shows for the loading case A the comparison between 3D FE results and the outcomes of the simplified models 1 and 2. No relevant differences can be noticed, although the hub motion is better reproduced by model 2, supporting the idea of neglecting soil non-linearity when the OWT is subjected to weak environmental loading. It is noteworthy that despite K_L is halved in model 2 with respect to model 1, a very similar frequency response is observed for the two models. Hence, the natural frequency seems to be mainly governed by the rotational stiffness and, as recently suggested by Arany *et al.* [16, 17], lateral stiffness has only a minimal effect on it.

The performance of model 2 is further illustrated in Figs. 17-18 for the bounding cases A and C. Compared to case A, model 2 works less well in presence of substantial non-linearity (case C): model 2 provides a 3% overestimation of f_0 , whereas the hub displacements are inaccurate in both cyclic amplitude and global trend – no displacement accumulation can be in fact reproduced by the spring model. This shortcoming may only be remedied by acknowledging the dependence of spring stiffnesses on the loading amplitude.

Figure 19 testifies that improved simulation of the case C 3D response is achieved by means of the third simplified model, i.e. by setting the spring stiffnesses equal to $K_{L,C2}$ and $K_{R,C2}$. The combined use of suitable viscous damping enables to capture reasonably well also the hub maximum displacement until about

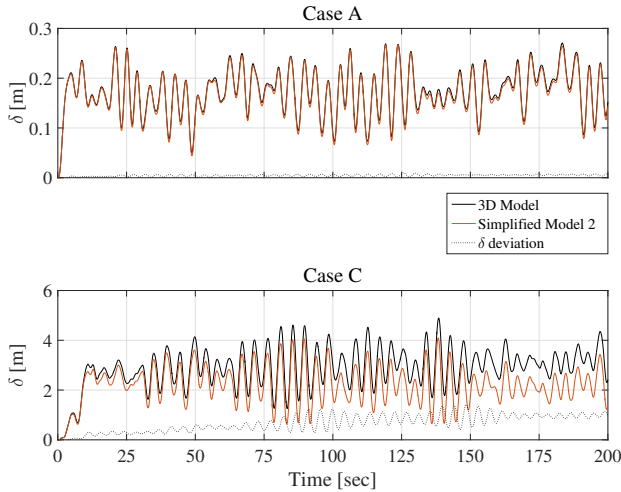


FIGURE 17. COMPARISON BETWEEN 3D AND SPRING MODEL 2 SIMULATIONS OF LOADING SCENARIOS A-C (TIME DOMAIN).

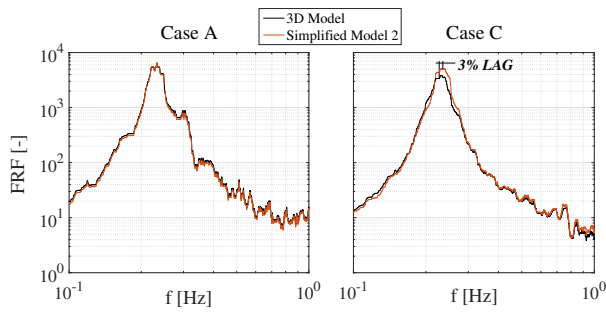


FIGURE 18. COMPARISON BETWEEN 3D AND SPRING MODEL 2 SIMULATIONS OF LOADING SCENARIOS A-C (FREQUENCY DOMAIN).

100 s – after that, significant displacement accumulation cannot be reproduced by a linear spring-dashpot model either.

CONCLUDING REMARKS

A 3D HM FE model was developed for the dynamic analysis of a standard 5 MW OWT on a monopile foundation in medium dense sand. Three different wind/wave loading scenarios were considered to explore the effects of the loading amplitude in the wind speed range from 5 to 20 m/s. Advanced FE modelling was exploited to account at the same time for slow soil dynamics, pore pressure effects and non-linear cyclic soil behaviour.

The FE results put in evidence the evolution of the foundational stiffness at increasing degree of mobilised soil plasticity. The OWT natural frequency varies with the load amplitude at

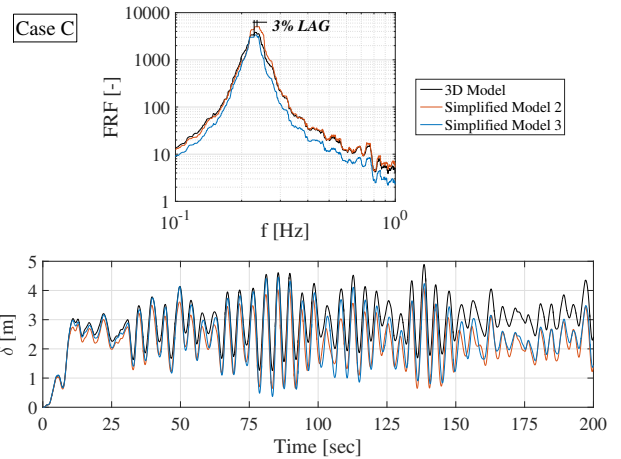


FIGURE 19. COMPARISON BETWEEN 3D AND SPRING MODEL 2-3 SIMULATIONS OF LOADING SCENARIO C.

an unsteady decrease rate, most likely due to the occurrence of undrained cyclic mobility in (medium) dense sandy soils. The outcomes of 3D FE analyses were exploited to set up engineering soil-structure interaction models formed by translational and rotational lumped springs. The importance of using stiffness values consistent with the current load magnitude was acknowledged, possibly along with viscous damping for better simulation of strong vibrations. Nonetheless, displacement accumulation trends cannot be captured without resorting to plasticity modelling.

Future work along this research line will be devoted to investigate the influence of the load amplitude over a wider range of sand types, from loose to dense. For this purpose, sand modelling based on critical state soil mechanics will be adopted to naturally capture void ratios effects. More efforts will be spent to foster the transfer of geotechnical knowledge from advanced to engineering modelling in offshore wind applications.

ACKNOWLEDGEMENTS

F. Pisanò is grateful for the inspiring discussions with C. Erbrich (Fugro AG, Perth) during his visit to the Centre for Offshore Foundation Systems at the University of Western Australia (*Martin Fahey Visiting Fellowship 2016*).

REFERENCES

- [1] Pineda, I., Ruby, K., Corbetta, G., Mbistrova, A., and Ho, A., 2016. Wind in power–2015 European statistics. Tech. rep., EWEA, Brussels, Belgium.
- [2] DNV, 2014. Offshore Standard DNV-OS-J101–Design of Offshore Wind Turbine Structures. Tech. rep., Det Norske Veritas AS, Oslo, Norway.

- [3] Doherty, P., and Kenneth, G., 2012. “Laterally loaded monopile design for offshore wind farms”. In Proceedings of the ICE - Energy, Vol. 1, pp. 7–17.
- [4] van Kuik, G. A. M., Peinke, J., Nijssen, R., Lekou, D. J., Mann, J., Sørensen, J. N., Ferreira, C., van Wingerden, J. W., Schlipf, D., Gebraad, P., et al., 2016. “Long-term research challenges in wind energy—a research agenda by the European Academy of Wind Energy”. *Wind Energy Science*, **1**, pp. 1–39.
- [5] Mazzoni, S., McKenna, F., Scott, M. H., Fenves, G. L., and Jeremic, B., 2007. *OpenSees command language manual*. Pacific Earthquake Engineering Research Center, University of California, Berkeley.
- [6] Cuéllar, P., Mira, P., Pastor, M., Fernández Merodo, J. A., Baeßler, M., and Rücker, W., 2014. “A numerical model for the transient analysis of offshore foundations under cyclic loading”. *Computers and Geotechnics*, **59**, June, pp. 75–86.
- [7] Corciulo, S., Zanolì, O., and Pisanò, F., 2017. “Transient response of offshore wind turbines on monopiles in sand: role of cyclic hydromechanical soil behaviour”. *Computers and Geotechnics*, **83**, March, pp. 221–238.
- [8] Jonkman, J., Butterfield, S., Musial, W., and Scott, G., 2009. Definition of a 5-MW Reference Wind Turbine for Offshore System Development. Tech. rep., NREL, Golden, CO.
- [9] Hansen, M. O. L., 2008. *Aerodynamics of wind turbines*. Earthscan, London.
- [10] Pierson, W. J., and Moskowitz, L., 1964. “A proposed spectral form for fully developed wind seas based on the similarity theory of SA Kitaigorodskii”. *Journal of geophysical research*, **69**(24), pp. 5181–5190.
- [11] Morison, J. R., Johnson, J. W., and Schaaf, S., 1950. “The force exerted by surface waves on piles”. *Journal of Petroleum Technology*, **2**(5), pp. 149–154.
- [12] Vugts, J. H., van der Tempel, J., and Schrama, E. A., 2001. “Hydrodynamic loading on monotower support structures for preliminary design”. In Proceedings of EWEA Special Topic Conference on Offshore Wind Energy, Brussels, Belgium.
- [13] McGann, C. R., Arduino, P., and Mackenzie-Helnwein, P., 2015. “A stabilized single-point finite element formulation for three-dimensional dynamic analysis of saturated soils”. *Computers and Geotechnics*, **66**, pp. 126–141.
- [14] Yang, Z., and Elgamal, A., 2008. “Multi-surface cyclic plasticity sand model with Lode angle effect”. *Geotechnical and Geological Engineering*, **26**(3), pp. 335–348.
- [15] Adhikari, S., and Bhattacharya, S., 2012. “Dynamic analysis of wind turbine towers on flexible foundations”. *Shock and vibration*, **19**(1), pp. 37–56.
- [16] Arany, L., Bhattacharya, S., Adhikari, S., Hogan, S. J., and Macdonald, J. H. G., 2015. “An analytical model to predict the natural frequency of offshore wind turbines on three-spring flexible foundations using two different beam models”. *Soil Dynamics and Earthquake Engineering*, **74**, pp. 40–45.
- [17] Arany, L., Bhattacharya, S., Macdonald, J. H. G., and Hogan, S. J., 2016. “Closed form solution of Eigen frequency of monopile supported offshore wind turbines in deeper waters incorporating stiffness of substructure and SSI”. *Soil Dynamics and Earthquake Engineering*, **83**, pp. 18–32.